

MoS₂/MoO₃ Heterojunction: Dual Role of the Type II set-up and Band Gap Modulation of MoS₂ upon Lithium-Ion Intercalation

Raheel Hammad, Amar Kumar, Tharangattu N. Narayanan, and Soumya Ghosh**

Abstract:

In recent times photorechargeable metal ion batteries have garnered significant attention but the atomistic details of the mechanism of the charging process is still unknown. MoS₂/MoO₃, a type II semiconductor heterostructure, has been shown to function as photocathode where during discharge the lithium ion (Li-ion) intercalation happens mostly in MoS₂ layers. Photo-exposure leads to exciton formation and the type II set-up is supposed to generate spatially separated and longer-lived charge carriers. The Li intercalated MoS₂ is known to undergo a phase transition from the semiconducting (2H) to a metallic (1T') phase. Hence, the proposal of exciton formation and its separation in Li_xMoS₂ during photocharging needs closer inspection. In this study, with the help of density functional theory (DFT) based studies that is aptly supported by experimental data, it is shown that Li_xMoS₂/MoO₃ forms a type II heterostructure where the underlying band gap of Li_xMoS₂ is exposed due to dispersion of electron density onto MoO₃ upto a certain value of x. Further studies show that the type II arrangement is lost prior to the phase transition. In order to investigate the electronic structure and the phase transition upon lithiation in the explicit heterostructure, we introduced two unconventional computational schemes. The presence of the band gap and the ensuing type II arrangement in Li_xMoS₂/MoO₃ upto a certain concentration of the intercalated Li-ion justifies the possibility of the photocharging process. We believe that the general concepts explored in this study will be important in the rational design of type II heterostructures that can behave as photo-cathode materials in Li-ion batteries.

Keywords: Solar Battery; Density Functional Theory; Type-II Heterostructure, Phase Transition; Band Gap Change

Due to the structural stability and reversible lithium ion (Li ion) intercalation/de-intercalation abilities, layered materials like $\text{LiNi}_x\text{Mn}_y\text{Co}_z$ have been widely used in Li ion batteries as cathode where they exhibit large capacity and high voltage discharge plateau, sometimes at the expense of the electronic band gap.^[1-4] In contrast, studies on the photo-cathode materials with a band gap commensurate with the frequency of light in the visible region, have been significantly low.^[5-7] Traditionally, a type II heterojunction has been employed for photosensing and photocatalytic applications in order to efficiently separate the charge carriers that are generated upon photo-excitation.^[8-12] The efficiency of the type II set-up is critically dependent on the alignment of the band edges of the two materials that ensures proper dispersion of the excited electron on the conduction band (CB) of the material with the higher band edges to the CB of the other material.^[8,9,13] Hence, for a type II heterojunction to act as a photocathode, the bands of the two materials need to remain properly aligned *during the full discharge cycle of the battery*. In this study we investigate the changes in the electronic band structure of MoS_2 upon lithiation in a type II set-up with MoO_3 that has been recently demonstrated in a photochargeable Li ion battery.^[8]

Bulk MoS_2 in 2H phase (with 2 layers of hexagonal lattice stacked in AB fashion) displays an indirect band gap of ~ 1.3 eV while the 1T' phase (monolayer of distorted octahedral phase) is found to be metallic.^[14-16] The computed band structure of monolayer 1H- MoS_2 displays a direct band gap of ~ 1.65 eV while there is a small indirect band gap in 1T' monolayer.^[14] The band gap of layered MoS_2 can be engineered by chemical doping^[17] or employing external stimulus.^[18] Previous studies indicate that upon lithiation, MoS_2 becomes metallic irrespective of the initial phase (Figure S1).^[19,20] The metallization questions the photocharging mechanism, where exciton formation has to happen upon the absorption of light in the lithiated MoS_2 (Li_xMoS_2).^[8]

In order to understand the electronic structure of the MoS_2 (bilayer)^[21]/ MoO_3 (bulk) heterostructure, one needs to align the band edges between the two materials. The alignment requires computation of the valence band maxima (VBM) of the two materials relative to the vacuum in addition to their band gaps, which invariably involves calculation of band edges for a slab of finite number of layers. Incidentally, previous density functional theory (DFT)^[22] calculations indicated that layered $\text{MoS}_2/\text{MoO}_3$ combination forms a type III heterojunction if PBE functional^[23] is employed.^[24] In order to avoid this pitfall, we employed an artificial layering scheme (henceforth termed as 'uL') for MoO_3 to obtain the desired type II band alignment (Figure 1a,b). Alternatively, one can employ the natural layering for MoO_3 and still obtain a type-II alignment by computing the band gaps with a more accurate hybrid functional (HSE06) while using PBE+U+D3^[25,26] for all the other relevant quantities to estimate the valence band offset (VBO) (see SI for details).

In Figure 1(c,d), two different type-II band alignments between bulk MoO_3 and bilayer 2H- MoS_2 are shown, employing either the natural layering (and gap from HSE06) or the uL layering for MoO_3 .^[27,28] The corresponding alignments for Li_xMoS_2 with varying x , along with an estimate of the number of electrons that is present in the CB of Li_xMoS_2 , are shown in Figure 2. As can be seen, the number of electrons is equal to the number of Li-ions that are added to the system. These electrons in the CB of Li_xMoS_2 make this system metallic albeit the presence of an underlying band gap. In addition, it is clear from the graph(s) (Figure 2) that this underlying band gap decreases with increase in the lithium ion concentration due to dramatic stabilization of the conduction band minimum (CBM) while the changes in the VBM is comparatively smaller. Ultimately, the type II character is lost and hence, there cannot be any efficient photo-excitation beyond that point ($x = 0.33$, Figure 2a; $x = 0.25$, Figure 2b). In order to understand the origin of the lowering of the CBM, we have plotted the corresponding projected density of states (PDOS, Figure S3) where the total DOS is projected separately onto the two MoS_2 layers. The upper MoS_2 layer, where the Li ions are being added, shows a steady metallization whereas the band edges of the lower layer do not change appreciably. These plots indicate that the reduction in the underlying band gap is caused by the presence of Li induced gap states near the CB edges.

We hypothesize that for lithium ion composition less than 0.25 (Figure 2b), the electron density in the CB of Li_xMoS_2 will be transferred to the CB of MoO_3 , thus exposing the underlying band gap and hence, the system can be amenable to photo-excitation. In order to investigate the electron distribution in lithiated MoS_2 in conjunction with MoO_3 , we set-up an explicit heterostructure composed of MoS_2 and MoO_3 (SI, Figure S4). Here we show that the type II alignment can be achieved in the explicit heterostructure with the uL scheme for MoO_3 as opposed to chemical modifications^[24] of the natural layering. Note that this artificial scheme is employed only to understand the electron density distribution in a type II setting. The structure of the supercell and the corresponding PDOS are shown in Figure 3. The corresponding structure and PDOS of a representative lithiated MoS_2 system ($\text{Li}_2\text{Mo}_{40}\text{S}_{80}$) in conjunction with MoO_3 ($\text{Mo}_{48}\text{O}_{144}$ in the supercell) are provided in Figure S5. Integration of the DOS shows that two electrons are present in the combined conduction band of the heterostructure. Resolving the DOS onto PDOS and integrating it reveals that 1.12 electrons are transferred from the CB of lithiated MoS_2 to the CB of MoO_3 .

While monolayer 1H-MoS₂ is more stable than 1T'-MoS₂,^[14,20] the stability order switches upon Li-ion intercalation beyond a certain Li ion concentration as shown in Figure S6.^[14] We wanted to investigate whether the transition point changes in a type-II set-up. This aspect is very important because if the structure transitions to the metallic phase at a very low concentration of lithium then the whole argument regarding lithium induced band gap modulation of the H-phase becomes inconsequential towards the photo-cathode behavior. Moreover, previous studies have shown that the phase stability can change depending on the number of electrons present in the system.^[14] Computing the energy of the two phases in an explicit heterojunction set-up, however, is not practically feasible since there is a significant lattice parameter mismatch between the 1T'-MoS₂ and MoO₃ structures.

In order to mimic the effect of the MoO₃ layers, we introduced a hypothetical layer of electronegative fluorine atoms on top of the lithiated MoS₂ surface (Figure S7) to extract electron density from the CB of lithiated MoS₂ in either phase without affecting the band edges (Figure S8). The amount of charge extracted by the fluorine sheet, obtained by integrating the differential PDOS, varies from 0.92e to 1.64e as the number of Li-ions is increased from 1 to 6 in a simulation cell with 12 units of MoS₂ (Table S1). The corresponding PDOS plots are shown in Figure S9. Using this set-up, we can compute the effect of the charge density extraction on the phase transition between the 2H- and the 1T'- phases upon lithiation. As shown in Figure 4, the transition point is shifted towards higher lithium composition.

In order to experimentally investigate the effects of lithiation in the metallization and phase transition of monolayer (1H) MoS₂, we have systematically studied lithiation/delithiation using *in situ* Raman spectroscopy [details in the supporting information]. As shown in Figure 5a, pristine MoS₂ exhibits two prominent peaks at ~383 cm⁻¹ and ~402 cm⁻¹, which correspond to the E_{12g} and A_{1g} vibration modes of monolayer 1H-MoS₂, respectively.^[29] On the other hand, the metallic 1T' phase is characterized by J1 and J2 modes centered at ~154 cm⁻¹ and ~225 cm⁻¹.^[30,31] The evolution of the vibrational modes of the 1H phase at different stages of charging is shown in Figure 5b. We performed UV-VIS absorption for pristine MoS₂ and Li_xMoS₂ (discharged till 1V). As shown in Figure S11, pristine MoS₂ shows absorption peaks at 660 nm, 610 nm, and 434 nm corresponding to A, B, and C exciton of 1H MoS₂,^[32] whereas Li_xMoS₂ does not show any absorption peak but higher absorption in the entire spectral range, indicating metallization upon lithiation. To understand the metallization of the 1H-phase upon lithiation, we performed *in situ* photoluminescence (PL) studies (Figure 6). The drastic decrease in intensity upon lowering the discharge voltage indicates decrease in efficiency of charge transfer from MoS₂ (lithiated) to MoO₃ and the shift in frequency to longer wavelengths imply decreasing band gap. Subsequent disappearance of photoluminescence below 2.95 V (during discharge) suggests disappearance of the type II character and phase transition to the 1T'-phase, which is also corroborated by the appearance of J1 and J2 peaks at that voltage in the Raman spectra. Additional graphs at different stages of charging / discharging are provided in the SI.

In this communication, we have explored the changes in the electronic band structure of MoS₂ upon lithiation in a type II heterojunction set-up with MoO₃. Our results suggest that (1) the type II arrangement exposes the underlying band gap of the otherwise metallic Li_xMoS₂ and (2) the band gap of 2H/1H-phase of Li_xMoS₂ reduces upon increasing x and eventually the type II band alignment is lost (~ x > 0.25). The loss of the type II character would suppress the photo-cathode behavior since the photoexcited electron-hole pair cannot be separated efficiently anymore. Computationally, the transition from the 2H/1H phase to the 1T' phase is found to occur after the loss of the type II character. We believe that the dual role of the type II set-up (exposure of the underlying band gap and efficient formation of charge separated excitons upon photoexcitation) is a general phenomenon. On the other hand, the current study suggests that one should also consider the band structure modulation upon Li-ion intercalation as an important gauge for an ideal photocathode material.

Figures

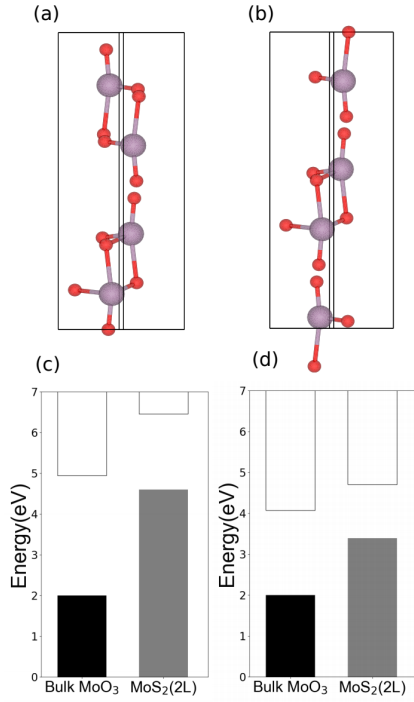


Figure 1: Unit cell for (a) conventional layering and (b) uL scheme. Band alignment between bilayer 2H-MoS₂ and bulk MoO₃ where VBO is computed with PBE+U whereas the band gap is computed either with HSE06 for the conventional layering of MoO₃ (c) or with PBE+U for the uL scheme of MoO₃ (d).

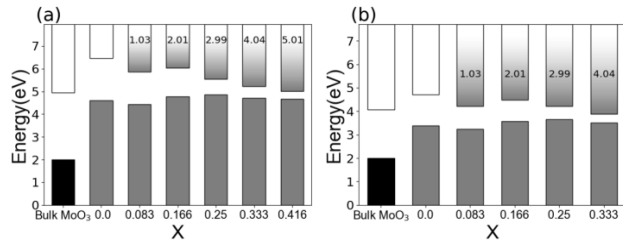


Figure 2: Band edges of Li_xMoS₂ for different values of x with the computational schemes shown in figures 1c and 1d, respectively. The type-II character is lost for x > 0.33 and x > 0.25 in the two cases respectively.

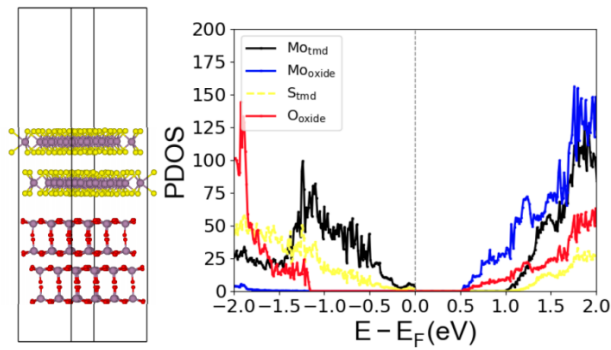


Figure 3: Left: Supercell for 2H-MoS₂/MoO₃ (uL) heterostructure Right: Corresponding PDOS resolved into Mo (MoS₂, black), Mo (MoO₃, blue), S (yellow), O (red) density of states.

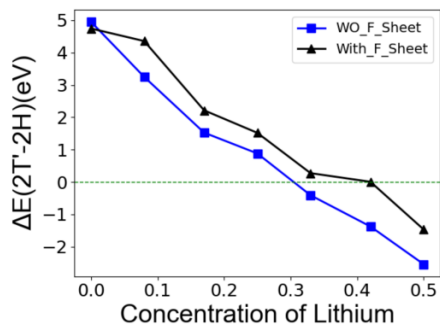


Figure 4. Phase transition with or without the hypothetical F6 sheet.

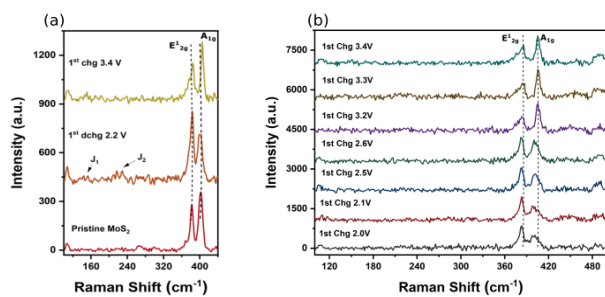


Figure 5. The *in situ* Raman spectra of monolayer based electrodes during Lithiation/delithiation (with Lithium metal as the other electrode) at different voltage vs Li/Li⁺. (a) Initial (pristine) MoS₂ monolayer (Open circuit voltage: 2.8V), 1st discharge (dchg, 0.01 mAcm⁻²) at 2.2V and after over charging (chg) till 3.4V. (b) The spectra taken during the electrochemical charging at different charging potentials.

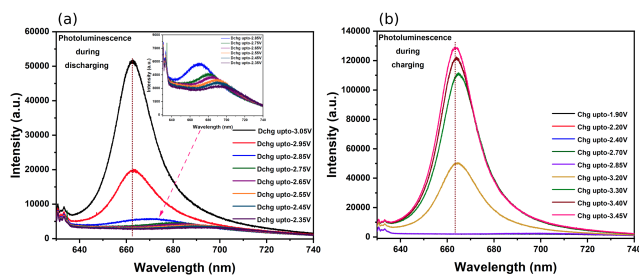


Figure 6: The *in situ* photoluminescence (PL) of MoS₂ monolayer based electrodes at different discharging voltages vs Li/Li⁺: (a) during discharging from charged state at 3.45 V till 2.35 V (inset PL curve shows discharge state from 2.85V to 2.35V). (b) During charging from discharged state 1.90 V to 3.45V.

ASSOCIATED CONTENT

Supporting Information

Experimental methods, additional plots, further details regarding band alignment

AUTHOR INFORMATION

Corresponding Authors

Soumya Ghosh – *Tata Institute of Fundamental Research – Hyderabad, 36/P, Gopanpally Village, Serilingampally Mandal, Ranga Reddy District, Hyderabad 500046, India*; Orchid ID: orcid.org/0000-0002-9429-5238; Email ID: soumya.ghosh@tifrh.res.in

Tharangattu N. Narayanan - *Tata Institute of Fundamental Research – Hyderabad, 36/P, Gopanpally Village, Serilingampally Mandal, Ranga Reddy District, Hyderabad 500046, India*; Orchid ID: orcid.org/0000-0002-5201-7539; Email ID: tnn@tifrh.res.in

Authors

Raheel Hammad - *Tata Institute of Fundamental Research – Hyderabad, 36/P, Gopanpally Village, Serilingampally Mandal, Ranga Reddy District, Hyderabad 500046, India*

Amar Kumar - *Tata Institute of Fundamental Research – Hyderabad, 36/P, Gopanpally Village, Serilingampally Mandal, Ranga Reddy District, Hyderabad 500046, India*

Notes

There is no competing financial interesting

ACKNOWLEDGEMENTS

The authors from TIFRH acknowledge the financial support from Department of Atomic Energy, Government of India, under Project Identification No. RTI 4007. TNN and SG would like to acknowledge the funding support from Infosys-TIFR “Leading Edge” Research Grant.

REFERENCES

- (1) Susai, F. A.; Kovacheva, D.; Chakraborty, A.; Kravchuk, T.; Ravikumar, R.; Talianker, M.; Grinblat, J.; Burstein, L.; Kauffmann, Y.; Major, D. T.; Markovsky, B.; Aurbach, D. Improving Performance of $\text{LiNi}_{0.8}\text{Co}_{0.1}\text{Mn}_{0.1}\text{O}_2$ Cathode Materials for Lithium-Ion Batteries by Doping with Molybdenum-Ions: Theoretical and Experimental Studies. *ACS Appl. Energy Mater.* **2019**, 2 (6), 4521–4534.
- (2) Morgan, L. M.; Islam, M. M.; Yang, H.; O’Regan, K.; Patel, A. N.; Ghosh, A.; Kendrick, E.; Marinescu, M.; Offer, G. J.; Morgan, B. J.; Islam, M. S.; Edge, J.; Walsh, A. From Atoms to Cells: Multiscale Modeling of $\text{LiNi}_x\text{Mn}_y\text{Co}_z\text{O}_2$ Cathodes for Li-Ion Batteries. *ACS Energy Lett.* **2022**, 7 (1), 108–122.
- (3) Dixit, M.; Markovsky, B.; Schipper, F.; Aurbach, D.; Major, D. T. Origin of Structural Degradation during Cycling and Low Thermal Stability of Ni-Rich Layered Transition Metal-Based Electrode Materials. *J. Phys. Chem. C* **2017**, 121 (41), 22628–22636.
- (4) Manthiram, A. A Reflection on Lithium-Ion Battery Cathode Chemistry. *Nat. Commun.* **2020**, 11 (1), 1–9.

- (5) Ahmad, S.; George, C.; Beesley, D. J.; Baumberg, J. J.; De Volder, M. Photo-Rechargeable Organo-Halide Perovskite Batteries. *Nano Lett.* **2018**, *18* (3), 1856–1862.
- (6) Boruah, B. D.; Wen, B.; De Volder, M. Light Rechargeable Lithium-Ion Batteries Using V_2O_5 Cathodes. *Nano Lett.* **2021**, *21* (8), 3527–3532.
- (7) Salunke, A. D.; Chamola, S.; Mathieson, A.; Boruah, B. D.; De Volder, M.; Ahmad, S. Photo-Rechargeable Li-Ion Batteries: Device Configurations, Mechanisms, and Materials. *ACS Appl. Energy Mater.* **2022**, *5* (7), 7891–7912.
- (8) Kumar, A.; Thakur, P.; Sharma, R.; Puthirath, A. B.; Ajayan, P. M.; Narayanan, T. N. Photo Rechargeable Li-Ion Batteries Using Nanorod Heterostructure Electrodes. *Small* **2021**, *17* (51), 2105029.
- (9) Kumar, A.; Hammad, R.; Pahuja, M.; Arenal, R.; Ghosh, K.; Ghosh, S.; Narayanan, T. N. Photo-Rechargeable Li Ion Batteries Using TiS_2 Cathode. **2023**. <https://doi.org/10.48550/arxiv.2301.06155>.
- (10) Das, R.; Sarkar, S.; Kumar, R.; Ramarao, S. D.; Cherevotan, A.; Jasil, M.; Vinod, C. P.; Singh, A. K.; Peter, S. C. Noble-Metal-Free Heterojunction Photocatalyst for Selective CO_2 Reduction to Methane upon Induced Strain Relaxation. *ACS Catal.* **2022**, *12* (1), 687–697.
- (11) Zhao, B.; Gan, Z.; Johnson, M.; Najafidehaghani, E.; Rejek, T.; George, A.; Fink, R. H.; Turchanin, A.; Halik, M. 2D van Der Waals Heterojunction of Organic and Inorganic Monolayers for High Responsivity Phototransistors. *Adv. Funct. Mater.* **2021**, *31* (42), 2105444.
- (12) Liu, X.; Gu, J.; Ding, K.; Fan, D.; Hu, X.; Tseng, Y. W.; Lee, Y. H.; Menon, V.; Forrest, S. R. Photoresponse of an Organic Semiconductor/Two-Dimensional Transition Metal Dichalcogenide Heterojunction. *Nano Lett.* **2017**, *17* (5), 3176–3181.
- (13) Hu, C.; Chen, L.; Hu, Y.; Chen, A.; Chen, L.; Jiang, H.; Li, C. Light-Motivated SnO_2/TiO_2 Heterojunctions Enabling the Breakthrough in Energy Density for Lithium-Ion Batteries. *Adv. Mater.* **2021**, *33* (49), 2103558.
- (14) Kan, M.; Wang, J. Y.; Li, X. W.; Zhang, S. H.; Li, Y. W.; Kawazoe, Y.; Sun, Q.; Jena, P. Structures and Phase Transition of a MoS_2 Monolayer. *J. Phys. Chem. C* **2014**, *118* (3), 1515–1522.
- (15) Fleischauer, P. D. Fundamental Aspects of the Electronic Structure, Materials Properties and Lubrication Performance of Sputtered MoS_2 Films. *Thin Solid Films* **1987**, *154* (1–2), 309–322. .
- (16) He, K.; Poole, C.; Mak, K. F.; Shan, J. Experimental Demonstration of Continuous Electronic Structure Tuning via Strain in Atomically Thin MoS_2 . *Nano Lett.* **2013**, *13* (6), 2931–2936.
- (17) Suh, J.; Tan, T. L.; Zhao, W.; Park, J.; Lin, D. Y.; Park, T. E.; Kim, J.; Jin, C.; Saigal, N.; Ghosh, S.; Wong, Z. M.; Chen, Y.; Wang, F.; Walukiewicz, W.; Eda, G.; Wu, J. Reconfiguring Crystal and Electronic Structures of MoS_2 by Substitutional Doping. *Nat. Commun.* **2018**, *9* (1), 1–7.
- (18) Lanzillo, N. A.; O'Regan, T. P.; Nayak, S. K. Band Structure Modulation in MoS_2 Multilayers and Heterostructures through Electric Field and Strain. *Comput. Mater. Sci.* **2016**, *112*, 377–382.
- (19) Enyashin, A. N.; Seifert, G. Density-Functional Study of Li_xMoS_2 Intercalates ($0 \leq x \leq 1$). *Comput. Theor. Chem.* **2012**, *999*, 13–20.
- (20) Xia, J.; Wang, J.; Chao, D.; Chen, Z.; Liu, Z.; Kuo, J. L.; Yan, J.; Shen, Z. X. Phase Evolution of Lithium Intercalation Dynamics in $2H-MoS_2$. *Nanoscale* **2017**, *9* (22), 7533–7540.
- (21) Bilayer model allows increasing Li ion intercalation into MoS_2 without any explicit interaction between Li-Ion and MoO_3 .
- (22) Kohn, W.; Becke, A. D.; Parr, R. G. Density Functional Theory of Electronic Structure. *J. Phys. Chem.* **1996**, *100* (31), 12974–12980.

- (23) Perdew, J. P.; Burke, K.; Ernzerhof, M. Generalized Gradient Approximation Made Simple. *Phys. Rev. Lett.* **1996**, *77* (18), 3865–3868.
- (24) Shahrokhi, M.; Raybaud, P.; Le Bahers, T. 2D MoO_{3-x}S_x/MoS₂ van Der Waals Assembly: A Tunable Heterojunction with Attractive Properties for Photocatalysis. *ACS Appl. Mater. Interfaces* **2021**, *13* (30), 36465–36474.
- (25) Dudarev, S. L.; Botton, G. A.; Savrasov, S. Y.; Humphreys, C. J.; Sutton, A. P. Electron-Energy-Loss Spectra and the Structural Stability of Nickel Oxide: An LSDA+U Study. *Phys. Rev. B* **1998**, *57* (3), 1505–1509.
- (26) Grimme, S.; Antony, J.; Ehrlich, S.; Krieg, H. A Consistent and Accurate Ab Initio Parametrization of Density Functional Dispersion Correction (DFT-D) for the 94 Elements H-Pu. *J. Chem. Phys.* **2010**, *132* (15), 154104.
- (27) Li, Z.; Cao, F.; Wang, L.; Chen, Z.; Ji, X. A Novel Ternary MoS₂/MoO₃/TiO₂ Composite for Fast Photocatalytic Degradation of Rhodamine B under Visible-Light Irradiation. *New J. Chem.* **2019**, *44* (2), 537–542.
- (28) The combination of uL layering of MoO₃ combined with HSE06 gaps is discussed in SI, Figure S2.
- (29) Rani Sahoo, K.; Pradeep Chakravarthy, T.; Sharma, R.; Bawari, S.; Mundlia, S.; Sasmal, S.; Raman, K. V.; Narayanan, T. N.; Viswanathan, N. K.; Sahoo, K. R.; Sharma, R.; Bawari, S.; Mundlia, S.; Sasmal, S.; Raman, K. V.; Narayanan, T. N.; Chakravarthy, T. P.; Viswanathan, N. K. Probing Proximity-Tailored High Spin–Orbit Coupling in 2D Materials. *Adv. Quantum Technol.* **2020**, *3* (9), 2000042.
- (30) Zhu, Z.; Xi, S.; Miao, L.; Tang, Y.; Zeng, Y.; Xia, H.; Lv, Z.; Zhang, W.; Ge, X.; Zhang, H.; Wei, J.; Cao, S.; Chen, J.; Du, Y.; Chen, X.; Zhu, Z.; Tang, Y.; Zeng, Y.; Xia, H.; Lv, Z.; Zhang, W.; Ge, X.; Zhang, H.; Wei, J.; Cao, S.; Chen, X.; Xi, S.; Du, Y.; Miao, L.; Chen, J. Unraveling the Formation of Amorphous MoS₂ Nanograins during the Electrochemical Delithiation Process. *Adv. Funct. Mater.* **2019**, *29* (42), 1904843.
- (31) Hou, X.; Zhang, W.; Peng, J.; Zhou, L.; Wu, J.; Xie, K.; Fang, Z. Phase Transformation of 1T'-MoS₂ Induced by Electrochemical Prelithiation for Lithium-Ion Storage. *ACS Appl. Energy Mater.* **2022**, *5*(9), 11292–11303.
- (32) Wang, L.; Wang, Z.; Wang, H. Y.; Grinblat, G.; Huang, Y. L.; Wang, D.; Ye, X. H.; Li, X. Bin; Bao, Q.; Wee, A. S.; Maier, S. A.; Chen, Q. D.; Zhong, M. L.; Qiu, C. W.; Sun, H. B. Slow Cooling and Efficient Extraction of C-Exciton Hot Carriers in MoS₂ Monolayer. *Nat. Commun.* **2017**, *8*, 13906–13906.

Supplementary Information

MoS₂/MoO₃ Heterojunction: Dual Role of the Type II set-up and Band Gap Modulation of MoS₂ upon Lithium-Ion Intercalation

Raheel Hammad, Amar Kumar, Tharangattu N. Narayanan, and Soumya Ghosh**

Tata Institute of Fundamental Research – Hyderabad, 36/P, Gopanpally Village, Serilingampally Mandal, Ranga Reddy District, Hyderabad 500046, India

* To whom correspondence should be addressed: soumya.ghosh@tifrh.res.in; tnn@tifrh.res.in

Computational Details:

Our calculations employed density functional theory (DFT) in conjunction with PBE functional¹ as implemented in Vienna ab-initio simulation package (VASP)² with a plane wave basis set within the projector augmented plane-wave method (PAW)³. For all the MoS₂ calculations a kinetic energy cutoff for plane-waves was set to be 360 eV, while a cutoff of 500 eV was used for MoO₃ and MoO₃/MoS₂ heterostructure calculations. The energy and force convergence criteria were set to be 10^{-4} eV and $0.02 \text{ eV } \text{\AA}^{-1}$ respectively. We employed a gamma centered Monkhorst scheme of grid density 0.025 in each direction for all the calculations. We have used a Hubbard U parameter of 5.0 eV for both MoS₂ and MoO₃.^{4,5} For all multi layered systems DFT+U was combined with the dispersion correction (D3) by Grimme et.al⁶ to account for long range interactions. We relaxed the bulk and multi-layered geometry using PBE+U+D3 for MoS₂. Additionally HSE06 functional was used to compute the band gaps for a few systems as specified in the manuscript.

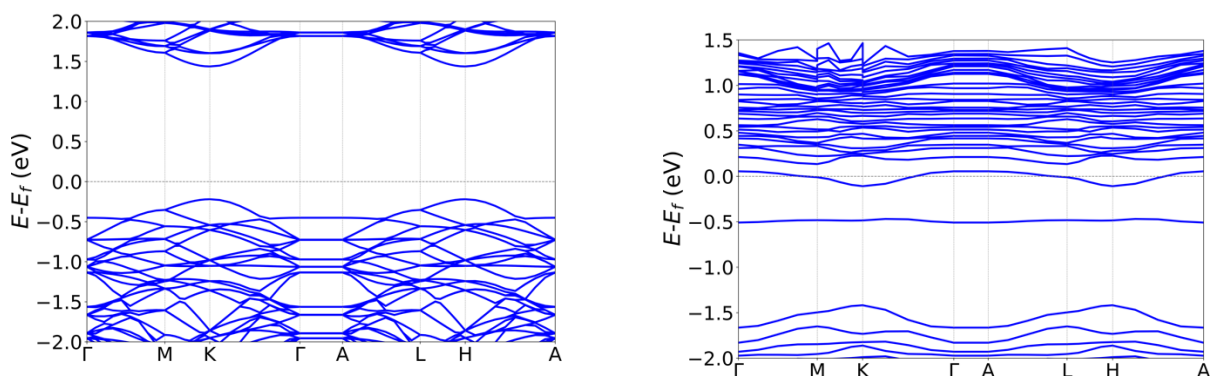


Figure S1: (a) Band structure of monolayer of 1H-MoS₂ computed with a periodic hexagonal cell with the lateral dimensions of 12.648 \AA (16 Mo and 32 S atoms) employing PBE+U functional (b) Computed band structure of monolayer of 1H-Li_{0.1875}MoS₂

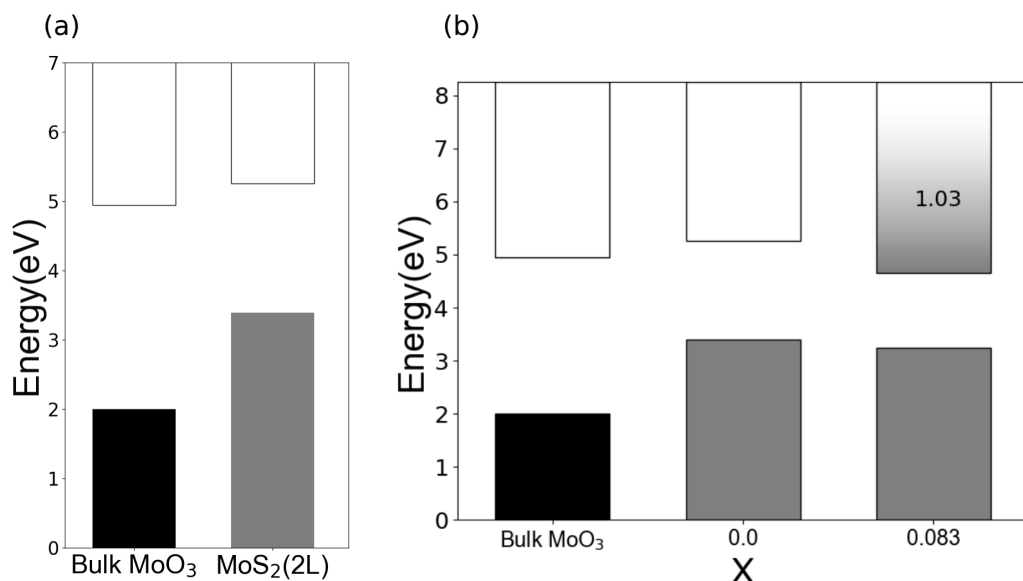


Figure S2. (a) Band gap is computed with HSE06 while the valence band offset computed with PBE+U within the uL scheme for MoO₃. (b) Change in band edges of lithiated MoS₂ as a function of Li-ion concentration. The type II alignment is lost for Li-ion concentration (x) less than 0.083

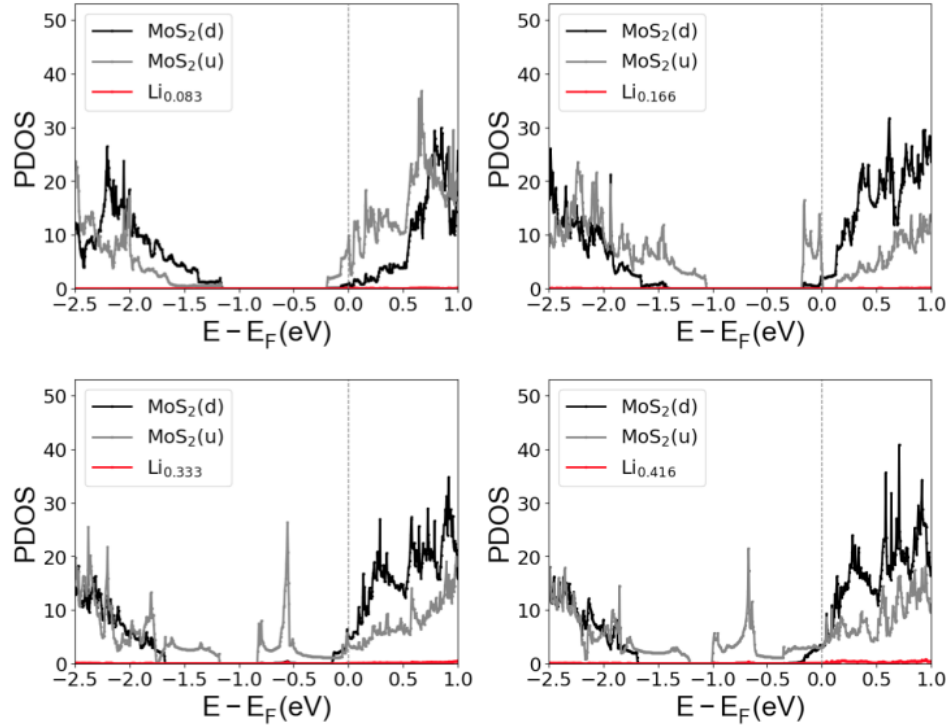


Figure S3. PDOS of lithiated MoS₂ for different concentration of Li-ion. The upper MoS₂ layer (MoS₂(u)) where the Li ions are added shows gradual metallization whereas the band edges of the bottom layer remains more or less unaffected. The analysis has been done with the PBE+U+D3 results.

MoS₂/MoO₃ Band-offset

We used planar averaged Hartree potential to compute the offset between MoO₃ and MoS₂. The valence band maxima (VBM) of bi-layer MoS₂(2L) is computed with HSE06 functional relative to its macroscopic average, which in turn is referenced to the vacuum level in a slab calculation. For bulk MoO₃ calculations (with HSE06), the VBM is referenced to the vacuum level using the following protocol. We first computed the electronic structure of multi-layered slabs of MoO₃ [010] in conjunction with vacuum in addition to the bulk MoO₃. The lateral dimensions of the slab and the bulk simulation cells are kept the same while the geometry was relaxed in both cases. Central layers in the slab are supposed to represent the bulk and using the macroscopic average of this region one can reference the VBM of the bulk to the vacuum.⁷⁻⁸ We can then compute the valence band offset (VBO) between the two materials. The simplified formula for the above method is given below

$$\begin{aligned} \text{VBO} &= \overline{\text{VBM}}_{2\text{MoS}_2} + \bar{V}_{2\text{MoS}_2-\text{vac}} - (\text{VBM}_{\text{MoO}_3} - \bar{V}_{\text{MoO}_3} + \bar{V}_{\text{MoO}_3} - \bar{V}_{\text{vac}}) \\ &= \overline{\text{VBM}}_{2\text{MoS}_2} + \bar{V}_{2\text{MoS}_2-\text{vac}} - (\overline{\text{VBM}}_{\text{MoO}_3} + \bar{V}_{\text{MoO}_3-\text{vac}}) \end{aligned}$$

\bar{V}_x = macroscopic average;

$\bar{V}_{x-\text{vac}}$ = macroscopic average of the bulk referenced to the vacuum;

$\overline{\text{VBM}}_x$ = VBM with respect to the macroscopic average

The conduction band offset is simply obtained by adding the band-gap to the VBM. However, PBE is known to underestimate the band gap, and therefore the experimental/HSE06 band gap can be combined with the above VBO for band alignment.^{8,9}

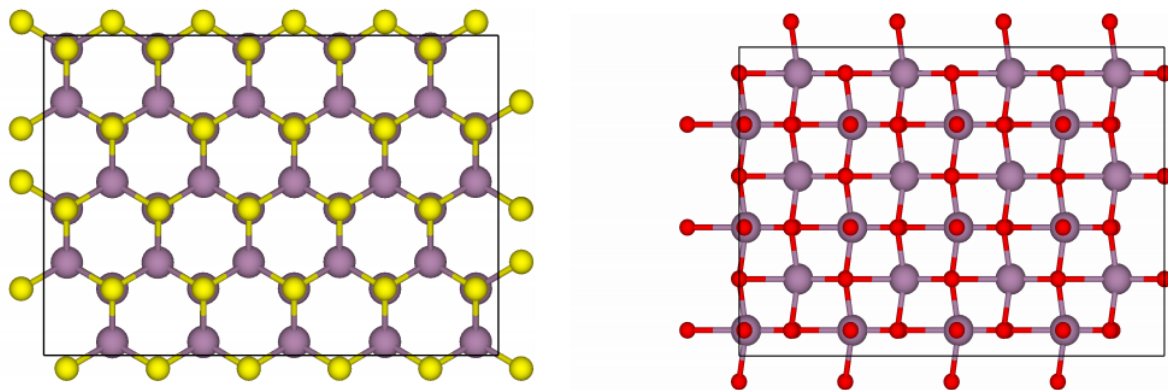


Figure S4. Units of MoS₂ [5x2](left) and MoO₃[4x3](right) employed in the explicit heterostructure calculations

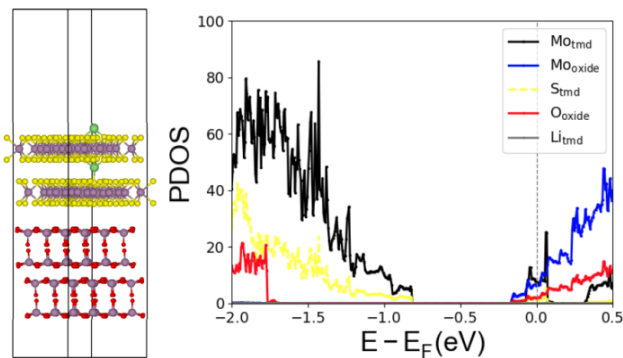


Figure S5. Left: Supercell of the explicit heterostructure with 2 Li-ions; Right: Corresponding PDOS projected separately on Mo(MoS₂), Mo(MoO₃), O, S, Li

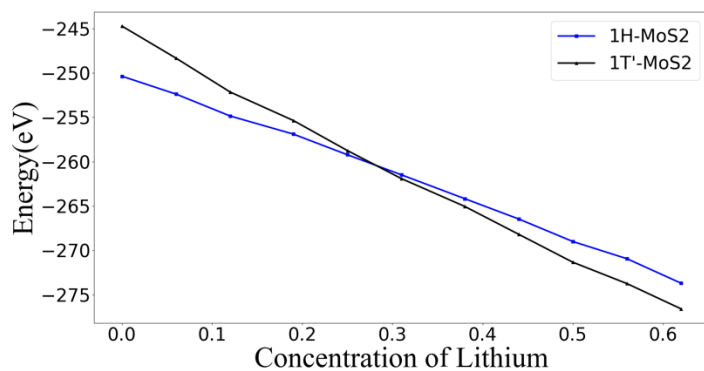


Figure S6. Phase transition in monolayer MoS₂ as a function of Li ion concentration for a periodic cell of 16 MoS₂ units. The simulation cell parameters for the hexagonal 1H and 1T' phases are 12.648 and 13.022 Å respectively. The energies are computed with PBE+U functional.

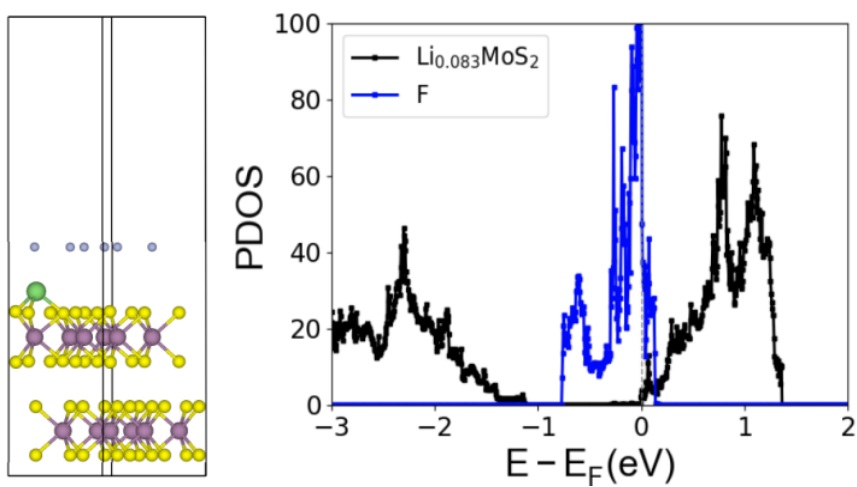


Figure S7. Left: Structure of $\text{Li}_{0.083}\text{MoS}_2$ + F6 sheet ; Right: Corresponding PDOS

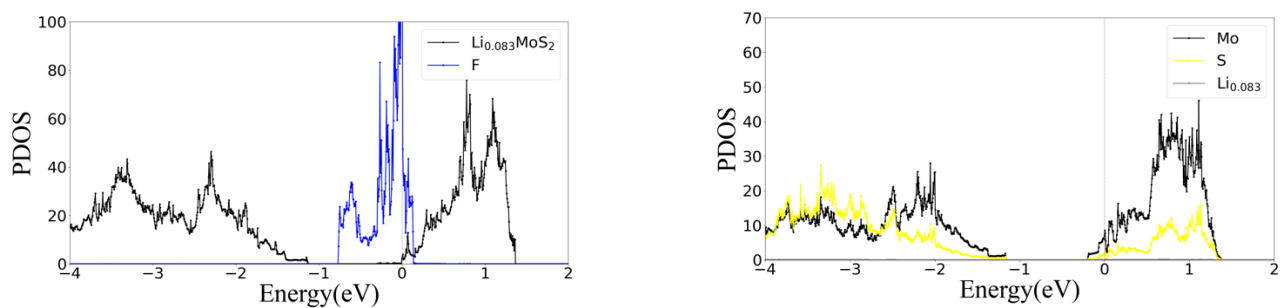


Figure S8. Left :PDOS of $\text{Li}_{0.083}\text{MoS}_2$ + F6 sheet; Right: PDOS of $\text{Li}_{0.083}\text{MoS}_2$

System	Charge Extracted by F-sheet
$\text{Li}_1\text{Mo}_{12}\text{S}_{24}/\text{F}_6$	0.920 e
$\text{Li}_2\text{Mo}_{12}\text{S}_{24}/\text{F}_6$	0.635 e
$\text{Li}_3\text{Mo}_{12}\text{S}_{24}/\text{F}_6$	1.601 e
$\text{Li}_4\text{Mo}_{12}\text{S}_{24}/\text{F}_6$	1.400 e
$\text{Li}_5\text{Mo}_{12}\text{S}_{24}/\text{F}_6$	1.321 e
$\text{Li}_6\text{Mo}_{12}\text{S}_{24}/\text{F}_6$	1.641 e

Table S1. Number of electrons extracted by the F6 sheet for different Li-ion concentrations

Integration of PDOS upto fermi level does not add up to total electrons in the system. To accurately compute the electron occupation number integration of total DOS has to be used. Incidentally, the PDOS of F and $\text{Li}_1\text{Mo}_{12}\text{S}_{24}$ (upto the Fermi level) do not overlap in $\text{Li}_1\text{Mo}_{12}\text{S}_{24}/\text{F}_6$ heterojunction. Therefore, the PDOS can be used to determine the integration limits and total DOS can be used to compute the electron occupations in fluorine and $\text{Li}_1\text{Mo}_{12}\text{S}_{24}$. To compute electron occupations in $\text{Li}_x\text{Mo}_{12}\text{S}_{24}/\text{F}_6$ for $x > 1$, we compute the integral of PDOS for F upto fermi level for these systems. This integral is then compared with PDOS integral for F in $\text{Li}_1\text{Mo}_{12}\text{S}_{24}/\text{F}_6$, the difference is used to determine the charge extracted by fluorine.

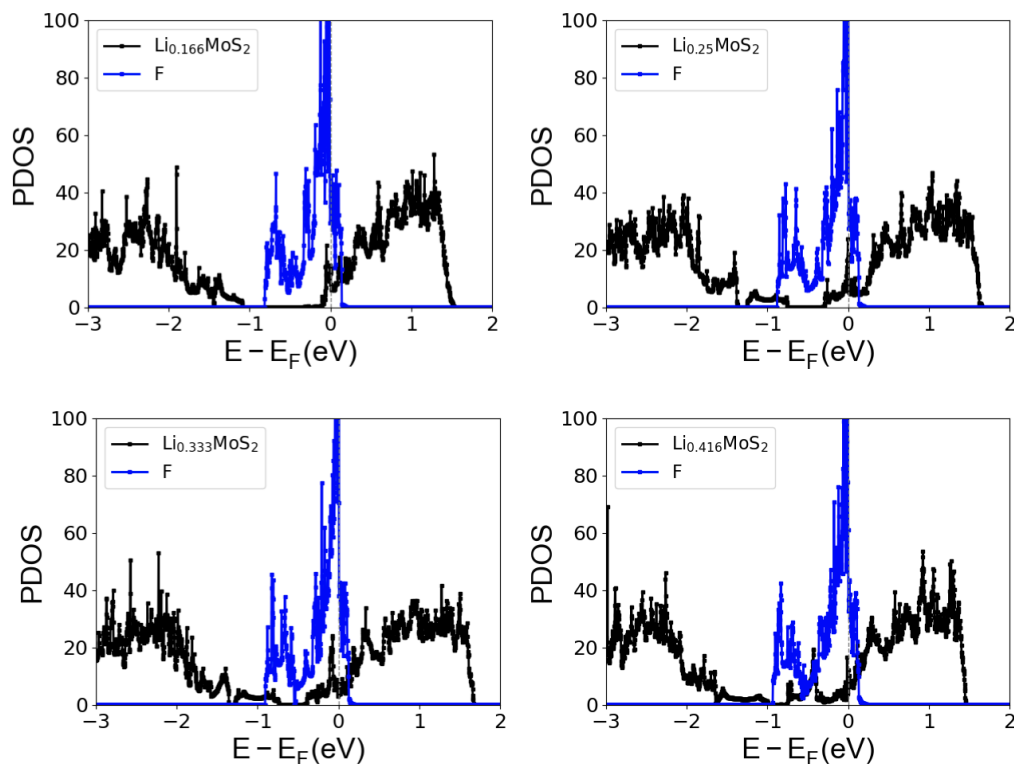


Figure S9. PDOS for different values of x in $\text{Li}_x\text{Mo}_{12}\text{S}_{24}/\text{F}_6$ system

Experimental Methods:

The growth procedure for MoS_2 monolayer synthesis involved the use of chemical vapor deposition (CVD) method. A two-zone furnace was employed for the growth, following a method previously discussed. Only MoO_3 and sulfur were used as precursors, and a small amount of NaCl was added to aid metal decomposition at lower temperatures. The process involved keeping sulfur at 210°C in Zone I and placing MoO_3 at 710°C in Zone II, as indicated in the schematic diagram. The experiment was conducted in the presence of 190 sccm N_2 , which acted as the carrier gas. Upon completion of the growth, the furnace was rapidly cooled to room temperature to prevent further multilayer growth.

Characterization:

The Renishaw Invia Raman spectroscopy was used to obtain in-situ and ex-situ Raman spectra and photoluminescence (PL) spectra. The analysis was conducted using a 532 nm exciton laser with a 20x objective. The laser power was optimized to prevent overheating and improve the noise to signal ratio of the data.

Electrochemical measurements:

Electrochemical measurements in this study were carried out using a single-channel Bio-logic potentiostat (SP-200). The electrochemical discharge measurements during the lithiation of monolayer MoS₂ were performed using a two-electrode battery setup consisting of an ITO-coated quartz electrode (25 mm × 25 mm) as the working electrode, lithium metal as the other electrode, and LiPF₆ in EC/EMC as the electrolyte. Prior to transferring the MoS₂ onto the ITO-coated quartz electrode, the electrode was thoroughly cleaned by washing it with soap and then with DI water and iso-propanol several times. The MoS₂ was first spin-coated with PMMA (0.204 g in 5 mL toluene) and then immersed in 2 M KOH overnight. The PMMA-coated MoS₂ was then transferred to water to remove KOH and subsequently transferred to the ITO-coated quartz electrode. The electrode was further cleaned with acetone after drying

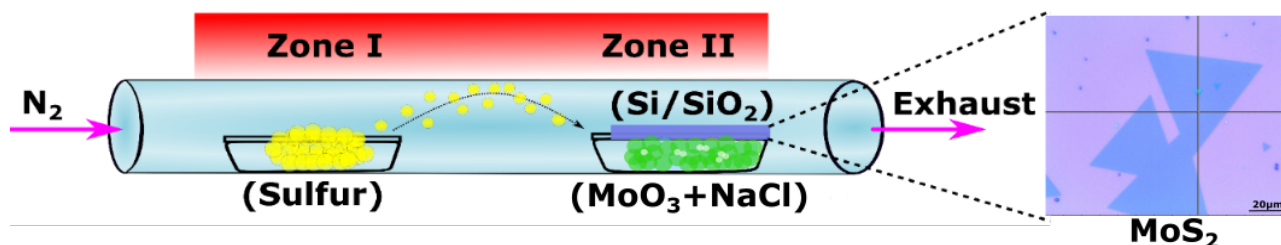


Figure S10. Schematic diagram of the MoS₂ growth by the CVD method. Sulfur is placed in Zone I whereas a mixture of MoO₃ and NaCl in Zone II. The MoS₂ on Si/SiO₂ is clearly seen in the optical image where the lateral size of the crystal is around 100-200 μm.

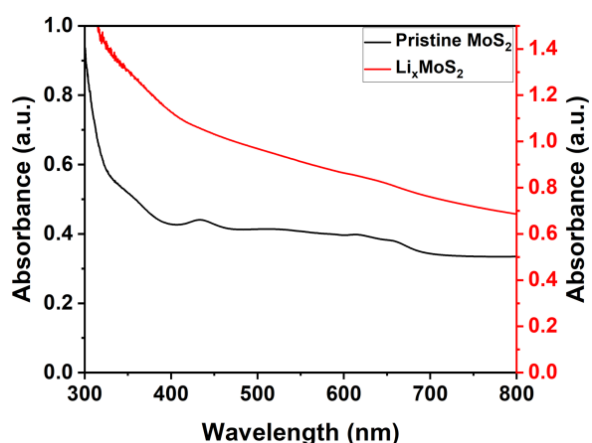


Figure S11: UV-Vis spectra of pristine and lithiated MoS₂

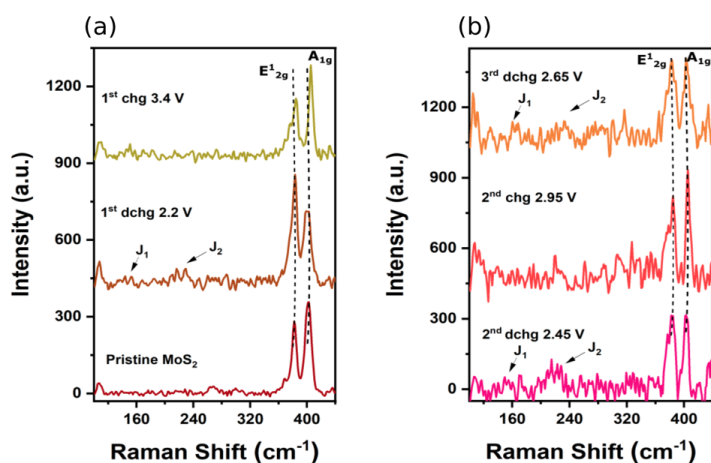


Figure S12: In-situ Raman spectra and Photoluminescence (PL) of MoS₂ monolayer based electrodes during Lithiation/delithiation (with Lithium metal as counter electrode) at different voltage vs. Li/Li⁺. (a) Initial MoS₂ monolayer, 1st discharge at 2.2V and after charging till 3.4V (b) 2nd discharge at 2.45V, 2nd charge at 2.95V and 3rd discharge at 2.65V.

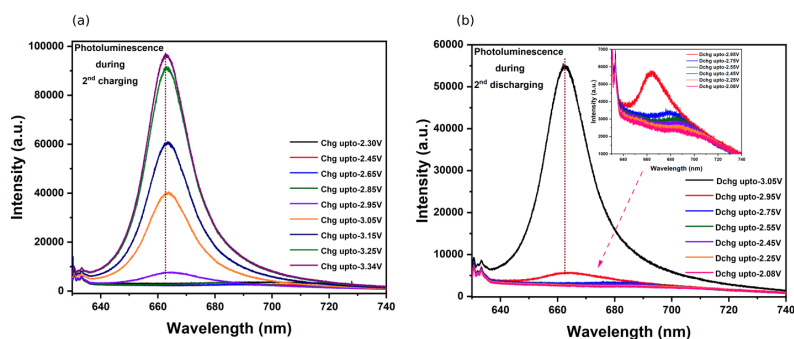


Figure S13: *In-situ* Photoluminescence (PL) of MoS₂ monolayer based electrodes during Lithiation/delithiation (with Lithium metal as counter electrode) at different voltage vs. Li/Li⁺. (a) PL during 2nd charging from discharged state 2.30V to charge till 3.34V (b) during discharging from charged state 3.05V to discharge till 2.08V (inset PL curve discharge state from 2.95V to 2.08V).

References

1. Perdew, J. P.; Burke, K.; Ernzerhof, M. Generalized Gradient Approximation Made Simple. *Phys. Rev. Lett.* 1996, 77, 3865–3868.
2. Kresse, G.; Furthmüller, J. Efficient Iterative Schemes for *ab initio* Total-Energy Calculations using a Plane-Wave Basis Set. *Phys. Rev. B* 1996, 54, 11169–11186
3. Kresse, G.; Joubert, D. From Ultrasoft Pseudopotentials to the Projector Augmented-Wave Method. *Phys. Rev. B* 1999, 59, 1758–1775.
4. Yan-Hua Lei and Zhao-Xu Chen* DFT+U Study of Properties of MoO_3 and Hydrogen Adsorption on $\text{MoO}_3(010)$, *J. Phys. Chem. C* 2012, 116, 49, 25757–25764
5. S. L. Dudarev, G. A. Botton, S. Y. Savrasov, C. J. Humphreys, and A. P. Sutton *Phys. Rev. B* 57, 1505
6. Stefan Grimme, Jens Antony, Stephan Ehrlich, and Helge Krieg *J. Chem. Phys.* 132, 154104 (2010)
7. José C. Conesa “Computing with DFT Band Offsets at Semiconductor Interfaces: A Comparison of Two Methods” *Nanomaterials* 2021, 11, 1581
8. Hanlin Fu, Justin C. Goodrich and Nelson Tansu “Band alignment of ScAlN/GaN heterojunction”, *Appl. Phys. Lett.* 117, 231105 (2020)
9. Wenjuan Yang, a Yanwei Wen, “Interfacial charge transfer and enhanced photocatalytic performance for the heterojunction WO_3/BiOCl : first-principles study”, *J. Mater. Chem. A*, 2014, 2, 20770